Published by IOP Publishing for Sissa Medialab

Received: *April 19, 2024*
Accepted: *July 31, 2024*
Published: *August 12, 2024*

Towards a precise measurement of ^{157}Tb nuclear decay data: Sample purification using resonance ionization mass spectrometry

Dominik Studer,[a,b,c,*] **Dorothea Schumann,**[d] **Nadine Mariel Chiera,**[d] **Emilio Andrea Maugeri,**[d] **Tom Kieck,**[b,c] **Karsten Kossert**[e] **and Klaus Wendt**[a]

[a] *Institut für Physik, Johannes Gutenberg-Universität Mainz, Staudingerweg 7, 55128 Mainz, Germany*
[b] *Helmholtz-Institut Mainz, Staudingerweg 18, 55128 Mainz, Germany*
[c] *GSI Helmholtzzentrum für Schwerionenforschung GmbH, Planckstr. 1, 64291 Darmstadt, Germany*
[d] *Paul Scherrer Institut Villigen, Reaktorstrasse 111, 5313 Villigen PSI, Switzerland*
[e] *Physikalisch-Technische Bundesanstalt (PTB), Bundesallee 100, 38116 Braunschweig, Germany*

E-mail: d.studer@gsi.de

Abstract: In nuclear physics, ^{157}Tb emerges as a prime candidate for experiments aimed at elucidating neutrino mass constraints and at searching for sterile neutrinos. Despite its importance, ^{157}Tb exhibits highly uncertain values for its nuclear decay properties. A significant challenge in many efforts to measure such data lies in the simultaneous undesired presence of ^{158}Tb in the samples, which hinders precise activity determination. Mass separation emerges as a crucial method for obtaining pure ^{157}Tb specimens. This work outlines the production of an isotopically-pure ^{157}Tb sample through mass separation and ion implantation, using the RISIKO facility at the University of Mainz. The initial material was obtained from proton-irradiated Ta samples through radiochemical separation at the Paul Scherrer Institute. In total, a sample containing $8.7(9) \cdot 10^{12}$ atoms of ^{157}Tb was obtained. The efficiency of the mass separation and ion implantation was 13(2) %. The purified material served as the basis for new research endeavors at the Physikalisch Technische Bundesanstalt Braunschweig aiming at the determination of nuclear data for ^{157}Tb with significantly improved precision.

Keywords: Targets (spallation source targets, radioisotope production, neutrino and muon sources); Instrumentation for radioactive beams (fragmentation devices, fragment and isotope, separators incl. ISOL, isobar separators, ion and atom traps, weak-beam diagnostics, radioactive-beam ion sources); Mass spectrometers

*Corresponding author.

https://doi.org/10.1088/1748-0221/19/08/P08009

Contents

1 Introduction and motivation

Terbium-157 — similarly to ^{163}Ho — is currently among the radionuclides under consideration for potential future experiments aimed at constraining the neutrino mass or searching for sterile neutrinos [1]. Accurate knowledge of the nuclear properties of this isotope (such as the half-life, emission probabilities and associated decay scheme parameters, fractional electron-capture probabilities, as well as the Q-value) is crucial for designing and executing various experimental studies and for validating theoretical models. However, nuclear decay data such as the half-life of ^{157}Tb exhibit widely spread values and large uncertainties, as shown in table 1.

Table 1. Half-life values for ^{157}Tb available in literature.

Year	Half-life in years (a)	Authors	Comment
2016	71 ± 7	Nica [2]	Decay data evaluation; calculated from [3]
1983	99 ± 10	Beyer et al. [3]	Implantation at CERN ISOLDE ($4 \cdot 10^{12}$ atoms); Auger-, X-ray measurements
1964	150 ± 30	Fujiwara et al. [4]	Measurement of K-X-rays; number of nuclei estimated from ^{157}Dy decay
1964	280 ± 120	Grigor'ev [5]	Measurement of K-X-rays; number of nuclei estimated from ^{157}Dy decay
1963	160 ± 40	Iwata et al. [6]	Na(Tl) measurement of photons; number of nuclei estimated from ^{157}Dy decay

In the most recent data evaluation [2], a half-life of 71(7) a is reported. This value was derived from the partial half-life for the K-electron-capture, $T_{1/2}(K-\text{capture}) = 455(40)$ a, experimentally determined by Beyer et al. [3], and from the calculated fractional electron-capture probability $P_K = 0.157(7)$, which is in turn based on a Q-value of 60.04(30) keV [7]. However, in their data analysis, Beyer et al. used a different $P_K = 0.218$, assuming a Q-value of 62.9(7) keV, which led to a

2024 JINST 19 P08009

half-life of $T_{1/2} = 99(10)$ a. These examples already highlight the importance of the K-electron-capture probability P_K, the determination of which relies heavily on the transition energy Q - a value that has not yet been directly measured but is considered for future experiments using Penning traps [8].

A first attempt to measure ^{157}Tb using Metallic Magnetic microCalorimeters (MMCs) was conducted as part of a Bachelor thesis at the Kirchhoff-Institute for Physics - Heidelberg University [9]. The measurements indicated the potential to determine the K/L ratio using MMCs. However, only quantum efficiencies well below unity could be achieved in the aforementioned pioneering work, and different models, which are now considered outdated, were used to derive the Q-value from the results. This situation also applies to the previously mentioned works, where P_K was calculated based on the Q-value. The situation highlights the urgent need for new experiments aimed at measuring radionuclide data with high accuracy and improved precision. Certain nuclide data, such as the transition probabilities of the two competing electron capture branches, the X-ray emission probabilities, and the probability for the capture of K-electrons, can be determined through the combination of precise activity measurements and photon spectrometry. The half-life can be experimentally determined through a combination of precise activity measurements and mass spectrometry, or through suitable long-term measurements. Corresponding experiments utilizing various liquid scintillation counting techniques [10] and γ-ray spectrometry are currently underway at the Physikalisch Technische Bundesanstalt (PTB) in Braunschweig, and some results have recently been published [11]. However, these experiments were only made possible by the availability of suitable ^{157}Tb samples, which, in addition to having a sufficiently high activity of more than 2 kBq, require high radionuclide purity. An impurity in the order of $A(^{158}\text{Tb})/A(^{157}\text{Tb}) = 10^{-3}$ would still be acceptable for an activity determination, though it would complicate the analysis and increase uncertainties. The complete absence of radioactive impurities in the final material was confirmed at PTB [11] thus ensuring best measurement conditions.

The main challenge faced during previous measurements at PTB was the concomitant presence in the sample of ^{158}Tb impurities - a radionuclide that is practically always produced alongside ^{157}Tb. With a half-life of about 180 years and several intense γ-ray lines, this radionuclide complicates the precise determination, particularly using liquid scintillation counting, of the activity of the electron-capture nuclide of ^{157}Tb, which emits only a few low-energetic γ-rays. Mass separation of $^{157/158}$Tb samples stands as one of the few options to obtain suitable ^{157}Tb samples in sufficient amounts with the required purity. In this work, we present the production of an isotopically pure ^{157}Tb sample achieved through mass separation and ion implantation using the RISIKO facility at the University of Mainz using a resonance ionization laser ion source. The combination of mass separation with a resonance ionization laser ion source provides high efficiency and therefore minimizes waste of valuable radioactive samples. Fedosseev et al. report an efficiency enhancement of > 1.8 using a three-step dye laser ionization scheme compared to a surface ion source in the case of terbium [12]. For other lanthanide elements efficiency enhancements of up to 60 are reported. In our case we chose a one-color, two-step ionization scheme, which is easy to implement by using a single laser and for which a total efficiency of 33(5) % was reported [13].

2 Experimental

2.1 Sample origin

Within the scope of the ERAWAST initiative, launched at Paul Scherrer Institut (PSI) approximately 20 years ago [14], activated components from the PSI accelerator facilities (such as samples from shielding,

2024 JINST 19 P08009

targets, or special irradiated specimens) are utilized to extract rare, scientifically interesting and urgently needed long-lived radionuclides through radiochemical separation. The Tb fraction described here, containing ^{157}Tb, originates from the reprocessing of highly radioactive tantalum samples obtained from the STIP-II project [15]. During that project, the tantalum samples were exposed to fluxes of high-energy protons and spallation neutrons with energies of up to 590 MeV at the SINQ facility of PSI. The detailed procedure for the dissolution of the tantalum samples is outlined in [16]. Subsequently, a series of ion-exchange separation processes were applied to obtain a purified Tb fraction in 1 M HNO_3. In this separation process, the γ-emitter ^{158}Tb ($T_{1/2}$ = 180(11) a, P_γ = 10 % at E_γ = 181.94 keV [17, 18]), which is also produced during the spallation of tantalum, served as an internal radiotracer. The method for separating and purifying the Tb fraction is described in detail in [19].

2.2 Mass-spectrometric analysis of the retrieved Tb sample

In order to determine the content of Tb isotopes in the sample, Sector-Field Inductively Coupled Plasma Mass Spectrometry (SF-ICP-MS) measurements were conducted utilizing a Thermo Fisher Element II® Sector-Field instrument. The Tb sample was initially diluted in 0.28 M HNO_3, prepared from high-purity nitric acid and Milli-Q® water. After preliminary measurements, a dilution factor of 100 was selected. This factor provided a suitable concentration of the isotopes of interest while allowing for the detection of other lanthanide impurities during background scanning. As an internal standard, a certified standard solution containing 10 mg L^{-1} Re was added (ESI, Elemental Scientific, Omaha, NE, U.S.A.). Concentrations of $^{157–159}$Tb in the solution were determined using an external multi-element standard (TraceCERT®, Periodic Table Mix 1, 2, and 3) dilution series. The SF-ICP-MS operation method was configured to scan masses between 116 and 187 in both low and medium resolutions. Details of instrument settings and data acquisition parameters are provided in table 2.

During the measurement sequence, the Tb sample was bracketed by the measurement of the multi-element standard dilution series. Each sample, along with every standard series, was preceded by an HNO_3-blank. To ensure accuracy, each measurement was repeated twice. The detection limit for each isotope was determined using three times the standard deviation of the blank measurements, taking into account the dilution factor of the samples. The intensities for each mass, measured in counts per second, were adjusted to account for machine background contributions by subtracting signals previously obtained from pure acid solutions. Internal normalization, utilizing ^{185}Re as an internal standard, was applied to mitigate any drift in machine responsiveness. Subsequently, the normalized count rate versus the concentration for each mass in the external multi-element standard series (measured both before and after the samples) was interpolated and utilized to calculate the concentration of each sample. The relative uncertainty of these concentrations is empirically estimated to be 10 % (2σ). This includes variations in standard measurements treated as samples, uncertainties in weighing during the preparation of the standard and sample solutions, as well as the uncertainty of the concentrations in the external standard ($\leq$ 0.8 %, 2σ).

2.3 Preparation of Tb samples for isotopic separation

A fraction of 70 mL of the retrieved Tb solution was concentrated to a volume of 10 mL through evaporation at 70 °C under a N_2 flow. Subsequently, 2 µL of the concentrated solution were drop-deposited onto a Zr foil (Alfa Aesar, thickness 25 µm, length 3 mm, height 3 mm). Four samples, namely A, B, C, and D, were prepared following the described procedure. The droplet deposited

2024 JINST 19 P08009

Table 2. Operating conditions and data acquisition parameters used for the ICP-MS measurements.

Inlet system	ESI SC-μ Autosampler with PTFE tubing MicroFlow PFA-ST nebulizer, uptake rate $\approx 70\,\mu L\,min^{-1}$ ESI PFA Conical Spray Chamber 2 mm Sapphire Injector tube with Quartz torch Nickel sampler and skimmer cones
Forward RF power	1350 W, guard electrode on
Ar gas flows	Cool gas: $16.5\,L\,min^{-1}$ Sample gas: $0.80\,L\,min^{-1}$ - $0.81\,L\,min^{-1}$ Auxiliary gas: $0.9\,L\,min^{-1}$ Additional gas: $0.20\,L\,min^{-1}$ - $0.22\,L\,min^{-1}$
Resolution	Low (LR) = 300 $m/\Delta m$ Medium (MR) = 4000 $m/\Delta m$
Data acquisition	Mass window: 50 % (LR); 60 % (MR) Search/Integration window: 80 % / 20 % Integration type: average Samples per peak: 20-30 Settling time: 0.001 s - 0.3 s
Detection mode	Analog and ion counting on secondary electron multiplier (SEM)
Measured masses	LR: 116 to 124; 134 to 170; 172 to 181; 185 and 187 MR: 134 to 170; 175; 177 to 181; 185 and 187
Number of scans	17
Measuring time per sample	6.00 min
Wash time between samples	10 min with 3 % HNO_3

on each Zr foil was allowed to dry in the air. Following this, γ-measurements of each Zr foil were conducted using a HPGe detector (Mirion) and the GENIE2000 software (see table 3). The activity of the Tb drop-deposited on each Zr foil was determined by comparing it with an inhouse-produced ^{44}Ti point-like reference source having an activity of 1280 Bq as of January 1st, 2018. All measurements were performed using the same sample geometry. The activity of the ^{44}Ti point-like reference source was calculated to be 1220 Bq on March 3rd, 2022, using the half-life for ^{44}Ti of 60 a, as provided in the JEFF 3.3 library. Each Zr foil was successively folded along its axis and inserted into the sample reservoir (see section 2.4).

2.4 Isotopic separation and ion implantation

The isotopic separation of ^{157}Tb/^{158}Tb and subsequent ion implantation were performed at the RISIKO mass separator in Mainz [20]. RISIKO is equipped with a laser ion source, operates at an acceleration voltage of 30 kV, conducts mass separation in a 0.6 T dipole magnet, and provides ion beam post-focalization onto an implantation target. An overview of the setup is given in figure 1.

The ion source consists of a sample reservoir (also known as mass marker), and an atomizer. The mass marker consists of a 2 mm outer diameter and 1 mm inner diameter tantalum capillary, which is

2024 JINST 19 P08009

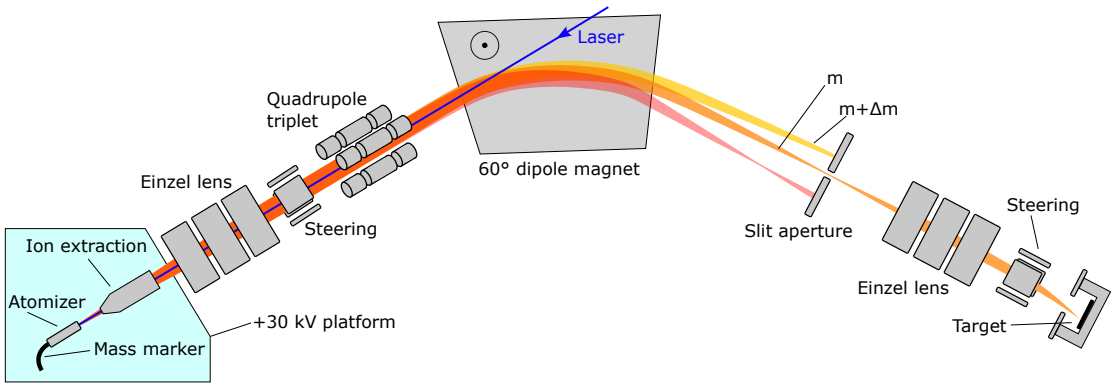

Figure 1. Schematic view of the RISIKO setup to implant ^{157}Tb. For details see text.

bent at a 90° angle over its length of 90 mm. It is connected to the atomizer, a 4 mm outer diameter and 2.5 mm inner diameter tantalum tube with a length of 35 mm. Both the mass marker and the atomizer can be independently heated by applying electric currents of up to 100 A and 300 A, respectively. The heating of the mass marker allows for the release of the sample into the atomizer. The latter is maintained at a temperature sufficiently high to ensure that the sample material exists as an atomic vapor. Additionally, thermionic electron emission from the hot atomizer surfaces provides a radially confining potential for positive ions and thus avoids losses due to re-neutralization at the walls [21]. This effect and corresponding ion load limitations in dependence of temperature were recently studied for a laser ion source and are discussed by Khwairakpam et al. [22]. Ionization occurs within the atomizer by irradiating the atomic vapor directly with pulsed lasers tuned to resonantly ionize the target element. A laser pulse repetition rate of 10 kHz ensures that each sample atom is irradiated by multiple laser pulses before exiting the atomizer due to thermal movement. Although the most probable velocity for a $m = 157$ u particle at 2000 °C is 50 mm/100 µs, the small diameter-to-length ratio of the atomizer leads to a mean free path which is in the order of the atomizer diameter, and consequently multiple wall collisions. The ions are guided out of the atomizer by the voltage gradient created by heating, and are finally accelerated to 10 keV by the extraction electrode located 40 mm downstream of the atomizer. The full beam energy of 30 keV is achieved at the first electrode of the Einzel-lens. Following beam shaping via the Einzel-lens and an electrostatic quadrupole triplet, the beam passes through a dipole magnet where ions are separated according to their mass-to-charge ratio. By adjusting the magnetic field strength appropriately, the desired mass value is transmitted through a slit aperture positioned at the focal plane of the magnet. The transmitted beam can be re-focused by another Einzel-lens onto the implantation target. A set of electrostatic steerer plates, along with the choice of aperture in front of the implantation target, enables spatial control of the implantation area. The beam current can be monitored either on a retractable Faraday-Cup located behind the slit aperture or directly on the implantation target, which is placed inside a Faraday-Cup.

Prior to working with the radioactive $^{157/158}$Tb samples, optimization of the laser ionization and separator operation parameters was conducted using a sample of approximately $3 \cdot 10^{13}$ atoms of stable ^{159}Tb. This stable Tb sample was prepared from an atomic absorption standard solution (Alfa Aesar, Specpure 1000 µg mL^{-1}), which was diluted with distilled water by a factor of 300. Subsequently, 3 µL of this solution were dried on a Zr foil following the procedure described in section 2.3, and then introduced in the mass marker. Here, Zr serves as a reduction agent and by fully enclosing the

2024 JINST 19 P08009

dried Tb solution prevents the release of terbium oxide, which is not ionized by the laser. The mass marker was crimped close in the middle, preventing released atoms from diffusing to the colder region close to the water-cooled current feedthrough. The Zr foil containing the drop-deposited sample was inserted and pushed close to the crimp site. Before heating the mass marker, the atomizer was heated with a power of 400 W. While the temperature was not directly measured, it was estimated to be close to 2000 °C, well above the melting point of Tb of 1356 °C. The corresponding Tb vapor pressure was therefore sufficiently high to prevent atoms from sticking to the cavity walls and the atomizer provided a radial ion confinement, as discussed above. Afterwards, the mass marker was slowly heated to release atomic Tb into the atomizer. The ionization of Tb atoms was achieved through a one-color, two-photon laser ionization scheme. Atoms were excited from a thermally populated state at $462\,\mathrm{cm}^{-1}$ to an intermediate state at $25\,076\,\mathrm{cm}^{-1}$, and finally to an autoionizing state at $49\,690\,\mathrm{cm}^{-1}$. Details of the laser ionization scheme can be found in [13], where the authors report an efficiency (meant as detected ions/sample atoms) of 33 %. The thermal population of the state at $462\,\mathrm{cm}^{-1}$ is approximately 20 % for $T > 500\,\mathrm{K}$ and relatively constant towards higher temperatures, as is also reported in [13]. Interestingly, this is a lower fraction than the reported efficiency. The dwelling time of atoms within the source has therefore be long enough for the ensemble to thermalize and repopulate this state. Consequently, the efficiency increase from additional lasers addressing e.g. the ground-state with a population of approximately 30 % at 2000 °C may be less than expected from thermal population alone. The laser light for the one-color, two-step resonance scheme, with a wavelength of 406 nm, was generated using a pulsed Ti:sapphire laser with intra-cavity second harmonic generation. The laser operated with a pulse length of 40 ns at a repetition rate of 10 kHz and an average power of 2 W at the entrance window of the vacuum chamber. The spectral line width was approximately 10 GHz, which was determined by measuring the fundamental emission of the laser with a wavelength meter (High Finesse WS6-600) and multiplying the result by $\sqrt{2}$. To achieve efficient ionization, the laser was focused inside the atomizer orifice. The optimal laser bandwidth can be estimated from Doppler broadening, which is in the order of 2 GHz in our case, and the width of the hyperfine structure. The latter can be determined by modeling the transition using the known hyperfine coupling constants $A(462\,\mathrm{cm}^{-1}) = 472.643(2)\,\mathrm{MHz}$, $A(25\,076\,\mathrm{cm}^{-1}) = 474.3(4)\,\mathrm{MHz}$, $B(462\,\mathrm{cm}^{-1}) = 1154.239(17)\,\mathrm{MHz}$ and $B(25\,076\,\mathrm{cm}^{-1}) = 659.6(17)\,\mathrm{MHz}$, which are reported in [23]. Note that these values were measured in ^{159}Tb, but are expected to be similar in ^{157}Tb due to the identical nuclear spin and similar nuclear moments. The resulting structure is approximately 10 GHz wide, with the most intense components located in an interval of $\approx$ 1 GHz at the center of the structure. In a resonance scan at a laser power of 2 W we measured a linewidth FWHM of 27 GHz, which is dominated by power broadening. Using the stable Tb test sample, an efficiency of 27 % was achieved. The ion signal enhancement on mass 159 due to the resonant laser was approximately two orders of magnitude.

For the implantation of ^{157}Tb, the Faraday cup in the implantation area was equipped with a 1 cm round aperture, and an aluminium foil (VWR International bvba, thickness 30 µm) was fixed and contacted inside the Faraday cup as the implantation target. The implantation target was located 21 mm behind the aperture. The ion beam was focused to a spot of approximately 1 mm diameter and then systematically scanned in a rectangular pattern across the 1 cm aperture by employing electrostatic steering plates. After mapping the aperture dimensions by measuring the ion current as a function of deflector voltages, the implantation process was started. An area within about 9.4 mm × 8.5 mm

2024 JINST 19 P08009

on the target (as later determined by autoradiography of the implanted Al foil; see section 2.5) was repeatedly scanned with the ion beam at a beam current ranging between 50 pA and 200 pA, with each scan lasting approximately 10 min. The sample foils endured between 1.5 h and 3 h before a significant drop in the ion current was observed. The relatively large scanning area was chosen to avoid sputtering losses of already implanted ions. Impinging ions possess the energy to sputter away a certain amount of atoms from the target surface, resulting in erosion of the aluminum foil within the implantation area. A detailed study of this effect is reported in [24], were also the case of terbium implantation is treated. Sputtering losses can be minimized by maximizing the beam energy, maximizing the implantation area, and by using a low-mass target material. For our case simulations employing the TRIDYN code [25] were conducted to estimate the influence of this effect, as well as additional losses arising from backscattering and transmission. According to the simulation results, the mean depth of terbium implantation into the target was 44 nm, with an depth spread full width at half maximum (FWHM) of 49 nm (see figure 2).

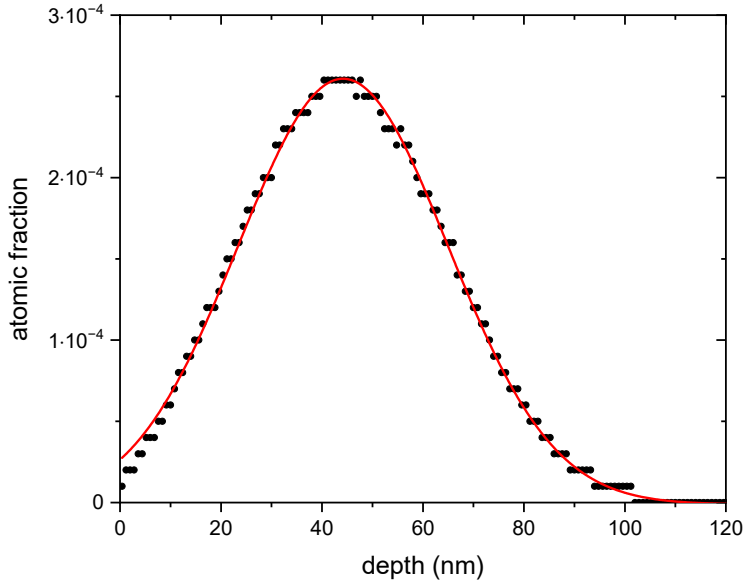

Figure 2. Depth profile of the Tb ion implantation into Al simulated with the TRIDYN code [25] (black dots). A normal distribution (red line) is fitted to the data, with a center of 44 nm and a FWHM of 49 nm.

Compared to this, only a negligible amount of the aluminum surface (less than one layer of atoms) is removed by sputtering. Therefore, the implanted terbium is only affected by the sputtering process at a 10^{-5} level. In total, 0.25 % of the impinging ions are lost, mostly due to backscattering from the target surface. The samples listed in table 4 were implanted in the order D, B, A, C.

2.5 Autoradiography

The distribution pattern of ^{157}Tb deposited on the substrate was analyzed using radiographic techniques. The sample was captured on a Fujifilm BAS-SR imaging plate, subsequently imaged using a GE Typhoon^{TM} FLA 7000 Imaging Plate Reader at a resolution of 25 µm per pixel. The resulting image was stored as a 16-bit TIFF file in greyscale. The exposure time was adjusted to maximize the dynamic range of greyscale data, aiming to avoid saturation while enhancing the image quality. The

2024 JINST 19 P08009

result is shown in figure 3. Note that the autoradiography measurement cannot distinguish between ^{157}Tb and ^{158}Tb, however, measurements using γ-ray spectrometry at PTB confirmed the purity as no radioactive impurity could be found [11].

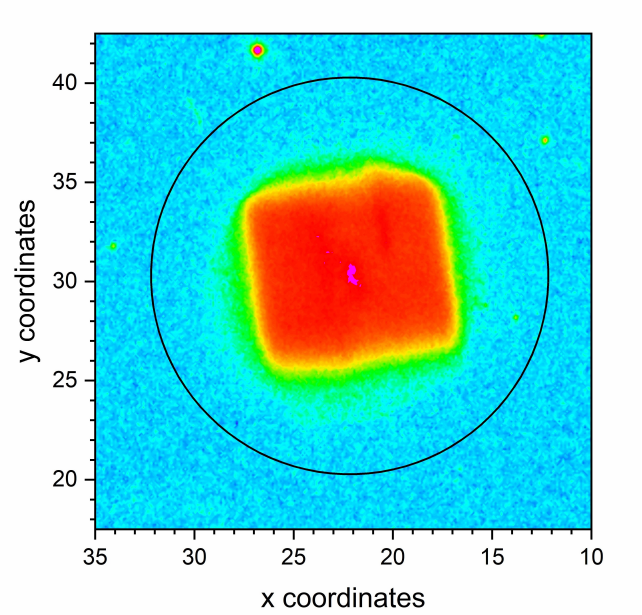

Figure 3. Autoradiographic image, showing the region of implanted ^{157}Tb atoms. Coordinates are given in millimeters. The size of the red area is 9.4 mm × 8.5 mm. In order to get rid of non-irradiated Al, the inner part was cut out, as indicated by the black circle.

2.6 Preparation of the isotopically pure Tb-157 sample for the LSC measurement at PTB

Based on the information gained by autoradiography (figure 3), the portion of the Al foil containing the implanted ^{157}Tb was cut out and sent to PTB for measurements using γ-ray and X-ray spectrometry to enable the first studies on the decay scheme of ^{157}Tb. After completion of these preliminary measurements, the foil was returned to PSI and placed in a vial (HDPE material, capacity 20 mL), to which 5 mL of concentrated HCl were added. The solution was maintained at 90 °C for 5 hours. The formation of a white/silver precipitate, possibly an Al_2O_3 protective layer on the Al surface, was observed. Therefore, the dissolution was carried on by addition of 1 mL of HNO_3, forming thus aqua regia with an approximate 3:1 HCl to HNO_3 ratio. After the complete dissolution of the Al implantation foil, the solution was evaporated to dryness at 70 °C under a N_2 flow. Subsequently, it was re-dissolved in concentrated HCl to ensure the transformation to the chloride form, followed by another round of evaporation to dryness at 70 °C under a N_2 flow. Finally, the solution was re-dissolved in 0.1 M HCl, and the weight was determined using a certified Mettler-Toledo XP56 balance (1 µg scale interval) in a room with a controlled temperature within 20 °C to 23 °C. Systematic uncertainties arising from the buoyancy difference between the calibration weight of the balance and the weighed solution are below 0.055 %. A gravimetrically determined aliquot of Tb was withdrawn from the ^{157}Tb master solution and transferred to a glass injection vial with a Pharmafix closure (6 mm depth, 13 mm aluminum closing cap, Butyl/Teflon® septum, WICOM GmbH).

2024 JINST 19 P08009

3 Results and discussion

The concentrations of $^{157-159}$Tb contained in the Tb sample analyzed by ICP-MS are presented in table 3, with a deduced ratio of ^{157}Tb/^{158}Tb = 4.7. From the measured activities of ^{158}Tb and the ^{157}Tb/^{158}Tb ratio measured by ICP-MS, the number of ^{157}Tb atoms drop-deposited on each Zr foil was deduced (table 4).

Table 3. Amounts of $^{157-159}$Tb per gram of solution contained in the retrieved Tb fraction, as deduced by ICP-MS analysis.

Isotope	Concentration (µmol/g)	Concentration (ppm)
^{157}Tb	0.00375	0.58855
^{158}Tb	0.00079	0.12449
^{159}Tb	0.00497	0.78939

Table 4. Measured ^{158}Tb activity on each Tb sample prepared for isotopic separation. The amount of ^{157}Tb, calculated from the ^{157}Tb/^{158}Tb ratio deduced by ICP-MS, is given as well.

Sample	Activity (Bq)	No. of ^{158}Tb atoms	No. of ^{157}Tb atoms
A	813	$6.66 \cdot 10^{12}$	$3.16 \cdot 10^{13}$
B	224	$1.84 \cdot 10^{12}$	$8.72 \cdot 10^{12}$
C	697	$5.71 \cdot 10^{12}$	$2.71 \cdot 10^{13}$
D	495	$4.06 \cdot 10^{12}$	$1.93 \cdot 10^{13}$

The Terbium-157 from samples B, A and C was successfully implanted into the Al foil, with efficiencies of 28 %, 23 % and 9 %, respectively. These efficiencies were determined by comparing the integrated current on the implantation target to the initial number of ^{157}Tb atoms from table 4. Note that these values are overestimated by up to 40 % when comparing to the total efficiency determined by activity measurement, as discussed below. The reason for the lower efficiency in sample C could not be determined. However, for sample D, no stable ion current could be achieved, and therefore no beam was directed to the implantation target. It was later discovered that a water-cooling failure of the ion source may have affected the performance of the separator.

Figure 4 illustrates the distribution of implanted ions as a function of electrostatic deflector voltage, where 1000 V corresponds to approximately 1 cm deflection on the aperture plane. According to the ion current measurements, the total number of implanted ^{157}Tb ions was $1.22 \cdot 10^{13}$. An uncertainty for this number was not estimated, since several error sources are unknown. Firstly it is based on the assumption that all implanted ions are ^{157}Tb. Although the ion signal enhancement from the laser is almost two orders of magnitude, a contribution of non-resonantly ionized species cannot be fully excluded. However, a contaminant of mass 157 u being resonantly ionized with the exact same resonance peak is unlikely. In a laser scan during the implantation of sample B, the laser was detuned by 0.6 cm^{-1} to either side of the resonance peak, resulting in a signal drop to a level of 15 %, which we can use as an upper limit of non-resonant contribution to the ion signal. Secondly, the systematic error on the total ion signal is unknown since the implantation Faraday Cup was not calibrated. Depending on the incident particle energy and mass, as well as the target material, there may be contributions

2024 JINST 19 P08009

from charged particle sputtering, in particular electrons. Although the implantation Faraday Cup was equipped with an electron repeller, this effect cannot be excluded.

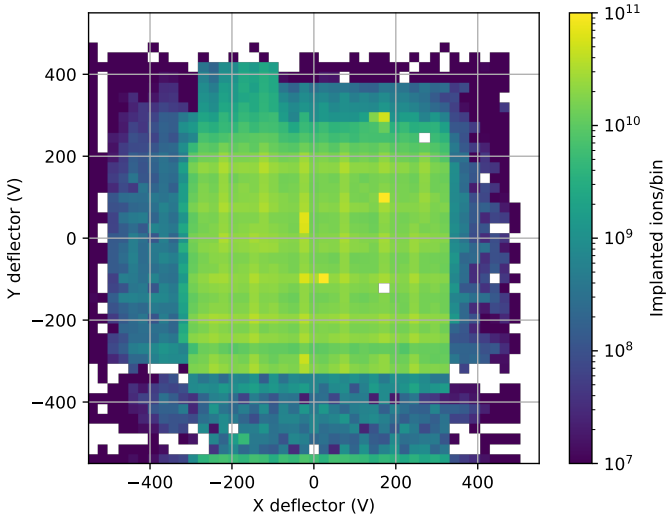

Figure 4. Amount of detected ions on the target Al foil. A voltage of 1000 V corresponds to approximately 1 cm deflection on the aperture plane (located 21 mm in front of the target plane). The ion beam was scanned in vertical rows from low to high voltage. Upon completing each row, the deflectors changed polarity before approaching the lowest set-point voltage of the next row. During this process, the picoamperemeter switched the measurement range, causing a slight lag in the readout, which resulted in an artificial signal in the lowest Y-row.

The sample obtained after dissolution of the Al implantation foil, referred to as "master solution", is a 0.1 M HCl solution with a mass of 3.356 14(11) g. Subsequently, an aliquot of 2.161 713(38) g of the master solution was shipped to PTB for various types of liquid scintillation counting measurements. The mass of the solution determined at PSI was confirmed by measurements at PTB. The activity concentration of the master solution was determined as 805.8(42) Bq g^{-1} [11]. With the total mass of the master solution and using the half-life of $T_{1/2}(^{157}\mathrm{Tb}) = 71(7)$ a from [2] this yields $N = T_{1/2} \cdot A/\ln(2) = 8.7(9) \cdot 10^{12}$. This value is approximately 40 % lower than the value obtained from ion current measurement. The total efficiency of the mass separation and ion implantation can be determined by N/N_{init}, using the initial number of ^{157}Tb atoms from table 4. If we disregard sample D, where no beam was directed to the target, the efficiency of the mass separation and ion implantation was 13(2) %.

The experiments aiming at an accurate determination of the γ-ray and X-ray emission probabilities and associated decay scheme parameters have been completed and are published in [11]. Additionally, a long-term measurement for the half-life determination of ^{157}Tb is still ongoing.

Acknowledgments

The authors would like to thank A. Fankhauser for the performance of the ICP-MS measurements and R. Dressler for the support with the γ-ray measurements. The work has been funded by the Swiss National Science Foundation under the project numbers 200020_178749 and 200020L_196959 and by the Deutsche Forschungsgemeinschaft under the number KO 2907/2-1.

2024 JINST 19 P08009

References

[1] D.K. Keblbeck et al., *Updated evaluation of potential ultralow Q-value β-decay candidates*, *Phys. Rev. C* **107** (2023) 015504 [arXiv:2201.08790].

[2] N. Nica, *Nuclear Data Sheets for A = 157*, *Nucl. Data Sheets* **132** (2016) 1.

[3] G.J. Beyer et al., *The Q Value of ^{157}Tb*, *Nucl. Phys. A* **408** (1983) 87.

[4] I. Fujiwara et al., *Decay of ^{157}Tb*, *Nucl. Phys.* **50** (1964) 346.

[5] E. Grigor'ev, *Half life of ^{157}Tb*, *Sov. Phys. JETP* **19** (1964) 770.

[6] S. Iwata et al., *The Half Life of ^{157}Tb*, *J. Phys. Soc. Jap.* **18** (1963) 315.

[7] S. Raman et al., *Unsuitability of ^{157}Tb for light neutrino rest mass studies*, *Phys. Rev. C* **46** (1992) 2241.

[8] M. Redshaw, *Precise Q value determinations for forbidden and low energy β-decays using Penning trap mass spectrometry*, *Eur. Phys. J. A* **59** (2023) 18.

[9] E. Pavlov, *Measurement of the calorimetric electron capture spectrum of ^{157}Tb using a metallic magnetic calorimeter*, B.Sc. thesis, KIP Heidelberg, Germany (2012).

[10] R. Broda, P. Cassette and K. Kossert, *Radionuclide metrology using liquid scintillation counting*, *Metrologia* **44** (2007) S36.

[11] J. Riffaud et al., *Determination of the activity and nuclear decay data of ^{157}Tb*, *Appl. Radiat. Isot.* **211** (2024) 111407.

[12] V. Fedosseev et al., *Ion beam production and study of radioactive isotopes with the laser ion source at ISOLDE*, *J. Phys. G* **44** (2017) 084006.

[13] V.M. Gadelshin et al., *Terbium Medical Radioisotope Production: Laser Resonance Ionization Scheme Development*, *Front. Med.* **8** (2021) 727557.

[14] D. Schumann, T. Stowasser, R. Dressler and M. Ayranov, *Possibilities of preparation of exotic radionuclide samples at PSI for scientific investigations*, *ract* **101** (2013) 501.

[15] Y. Dai et al., *The second SINQ target irradiation program, STIP-II*, *J. Nucl. Mater.* **343** (2005) 33.

[16] Z. Talip et al., *Radiochemical Determination of Long-Lived Radionuclides in Proton-Irradiated Heavy-Metal Targets: Part I — Tantalum*, *Anal. Chem.* **89** (2017) 13541.

[17] R.J. Prestwood et al., *Determination of the cross section for ^{159}Tb(n,2n) ^{158}Tb and the half-life of ^{158}Tb*, *Phys. Rev. C* **30** (1984) 823.

[18] N. Nica, *Nuclear Data Sheets for A = 158*, *Nucl. Data Sheets* **141** (2017) 1.

[19] N.M. Chiera, Z. Talip, A. Fankhauser and D. Schumann, *Separation and recovery of exotic radiolanthanides from irradiated tantalum targets for half-life measurements*, *PLoS One* **15** (2020) e0235711.

[20] T. Kieck et al., *Highly efficient isotope separation and ion implantation of ^{163}Ho for the ECHo project*, *Nucl. Instrum. Meth. A* **945** (2019) 162602 [arXiv:1904.05559].

[21] R. Kirchner, *On the Thermoionization in Hot Cavities*, *Nucl. Instrum. Meth. A* **292** (1990) 203.

[22] O.S. Khwairakpam et al., *The SPES laser ion source: Time structure, laser enhancement and efficiency measurements with gallium at ISOLDE Offline 2*, *Nucl. Instrum. Meth. B* **548** (2024) 165249.

[23] D. Stefanska and B. Furmann, *Hyperfine structure of the odd parity level system in the terbium atom*, *J. Phys. B* **50** (2017) 175002.

[24] M. Deseyn, *Maximizing the radionuclide collection efficiency at CERN-MEDICIS: A case study on terbium collections and sputtering*, M.Sc. theisis, KU Leuven, Leuven, Belgium (2023) [CERN-THESIS-2023-111].

[25] W. Möller, W. Eckstein and J.P. Biersack, *Tridyn-binary collision simulation of atomic collisions and dynamic composition changes in solids*, *Comput. Phys. Commun.* **51** (1988) 355.

2024 JINST 19 P08009